Appl. Phys. B (2016) 122:136
DOI 10.1007/s00340-016-6410-3

Applied Physics B
Lasers and Optics

Polarization dependence of plasmonic near-field enhanced photoemission from cross antennas

P. Klaer[1] · G. Razinskas[2] · M. Lehr[1] · X. Wu[2] · B. Hecht[2] · F. Schertz[1] · H.-J. Butt[3] · G. Schönhense[1] · H. J. Elmers[1]

Received: 30 July 2015 / Accepted: 11 April 2016 / Published online: 2 May 2016

Abstract The field enhancement of individual cross-shaped nanoantennas for normal incident light has been measured by the relative photoemission yield using a photoemission electron microscope. We not only measured the electron yield in dependence on the intensity of infrared light (800 nm, 100 fs), but also the polarization dependence. In the normal incidence geometry, the electrical field vector of the illuminating light lies in the surface plane of the sample, independent of the polarization state. Strong yield variations due to an out-of-plane field component as well as changes in the polarization state described by the Fresnel laws are avoided. The electron yield is related to the near-field enhancement as a function of the polarization state of the incident light. The polarization dependence is well explained by numerical simulations.

1 Introduction

The rapid progress in nanolithography has enabled the enhancement of light–matter interaction by tailored antenna structures [1–3]. Localized dipole plasmon modes excited in these antenna structures confine light on a nanoscale, and a gap size of the antenna much smaller than the resonant arm length results in a huge enhancement of the optical field. Theoretical [4–6] and experimental [7, 8] studies have led to a good understanding of the relevant localized dipole modes. In addition to linear polarization, circular polarization represents an interesting polarization state for enhanced near fields, because circularly polarized near fields concentrate angular momentum to a very small area, promoting catalytic chemical reactions [9], spectroscopic investigations [10], all-optical magnetic switching [11], and spin-polarized electron sources [12].

For circular polarization, Biagioni et al. [13] proposed a cross dipole antenna structure in analogy to the cross dipole antennas used for microwave technology, which transforms the incident electrical field to a near-field focus preserving the polarization state of the incoming wave. The proposed configuration [13, 14] is composed of four rectangular bars arranged as two dipole antennas sharing a gap. Accordingly, the enhanced localized field is confined in a focus of <50 nm. Although the cross dipole antenna fulfills the requirement of a polarized near field in simulations, fabrication of such a structure with high precision is still challenging keeping this field of research open to look for the most efficient way of manipulating the polarization.

In view of the potentially strong interaction, it is in particular an open question whether the polarized near-field enhancement of fabricated cross antennas can be described by the excitation of two arbitrary orthogonal dipole modes. The interaction of individual plasmon supporting structures, resulting from Coulomb forces between particles at sub-wavelength distance, leads to a rich variety of new coupled plasmon modes [5]. In addition to modes with a strong dipole moment maintaining a strong coupling to scattered light, coupled plasmon modes give rise to additional near-field modes without strong dipole moments having only a

This article is part of the topical collection "Ultrafast Nanooptics" guest edited by Martin Aeschlimann and Walter Pfeiffer.

✉ H. J. Elmers
elmers@uni-mainz.de

[1] Institut für Physik, Johannes Gutenberg-Universität Mainz, Staudingerweg 7, 55128 Mainz, Germany

[2] Institut für Physik, Julius-Maximilians-Universität, Am Hubland, 97074 Würzburg, Germany

[3] Max-Planck Institute for Polymer Research, Ackermannweg 10, 55128 Mainz, Germany

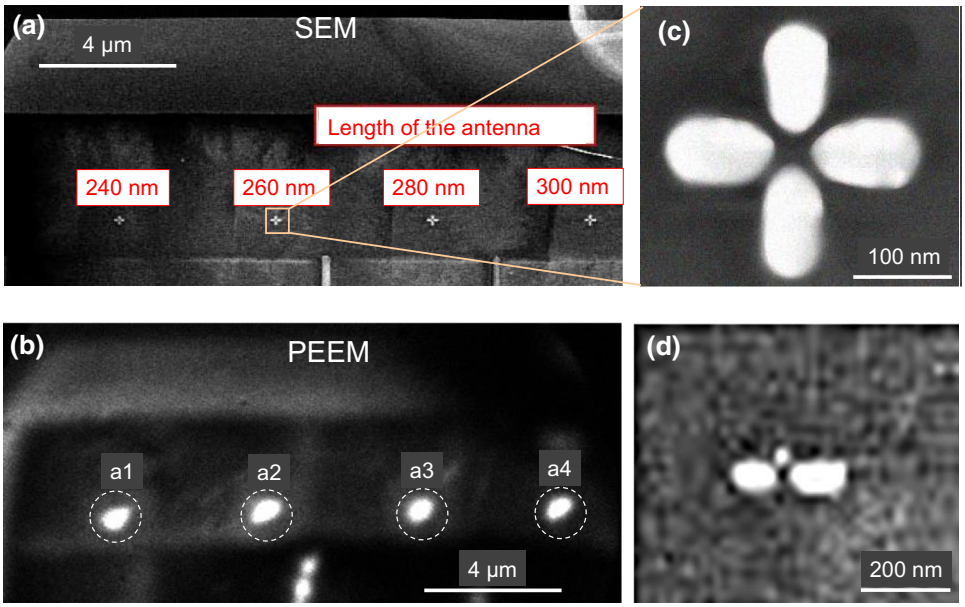

Fig. 1 **a** Scanning electron microscopy (SEM) image of cross-shaped nanoantennas a1–a4. A high-resolution SEM image of antenna a1 is shown in (**c**). **b** PEEM image ($h\nu = 1.55$ eV) showing the multi-photon photoemission yield of the same antennas (a1–a4) excited by circularly polarized light. The photoemission yields shown in Figs. 3, 4, and 6 result from an integration over the indicated circular areas. **c** Magnified SEM image of antenna a1. **d** SEM image of the two-arm antenna a5

weak coupling to the far field [15]. These dark modes have a longer lifetime due to the absence of a radiative decay channel providing a larger near-field enhancement [16, 17].

We investigated the cross-shaped structures shown in Fig. 1. In a previous publication [18], we could explain the polarization-dependent near-field enhancement for linear polarized light with numerical simulations considering the actual shape of the antennas. In this work, we discuss the dependence of the electron yield on the illuminating light intensity, and the lifetime of excited plasmon modes as determined by the autocorrelation function. The dependence on the polarization state of the incident light can be explained by a projection of the observed polarization dependence onto two independent orthogonal dipole modes.

2 Experimental

We fabricated cross antennas starting from single-crystalline gold flakes deposited on glass. The thickness of the Au flakes was approximately 80 nm (see Fig. 1). The glass was coated before by a layer of conductive indium tin oxide (ITO). A series of nanostructures was cut out of the flake using focused ion beam (FIB) milling. As a representative example, we describe here results obtained with five neighboring antennas on one sample. The design of the nanostructures roughly followed the proposition of Refs. [13, 14] with deviations from the ideal symmetric shape due to the limitations of the fabrication. The arm length of the structures increases from 240 to 300 nm. This interval includes the nominal resonance length for 800-nm excitation wavelength. The nominal resonance length is 275 nm calculated from the cross section of the wires and considering the dielectric constant of the substrate (see Ref. [18]). For comparison, we also show results for a single dipole antenna.

The near-field intensity is almost completely concentrated in the center of the nanostructures. The near-field intensity is related to the photoemission yield [18] that has been measured and analyzed here. The exciting laser wavelength of is 800 nm. The photoemission electron microscope (PEEM) is equipped with a two-dimensional delay-line detector allowing for the discrimination of individual nanoantennas while simultaneously measuring the electron yield of all nanoantennas in the field of view. The negligible dark count rate makes a background correction obsolete.

The experimental setup is illustrated in Fig. 2. A movable mirror switches between grazing incidence and normal incidence illumination. In the standard PEEM geometry, opaque samples can only be illuminated from the front at grazing incidence at an angle of 65° with respect to the surface normal because smaller angles are blocked by the objective lens. We performed measurements with normal incidence illumination which is facilitated by transparent substrates. In contrast to the grazing incidence, normal incidence conserves the incident polarization for all polarization states.

Excitation is performed by a beam of femtosecond laser pulses (100-fs pulse width, 80-MHz repetition rate, pulse energy 0.4 nJ, average laser power 32 mW) that was focused by an in situ singlet lens. The footprint of the laser beam on the surface is a circle with a beam diameter of

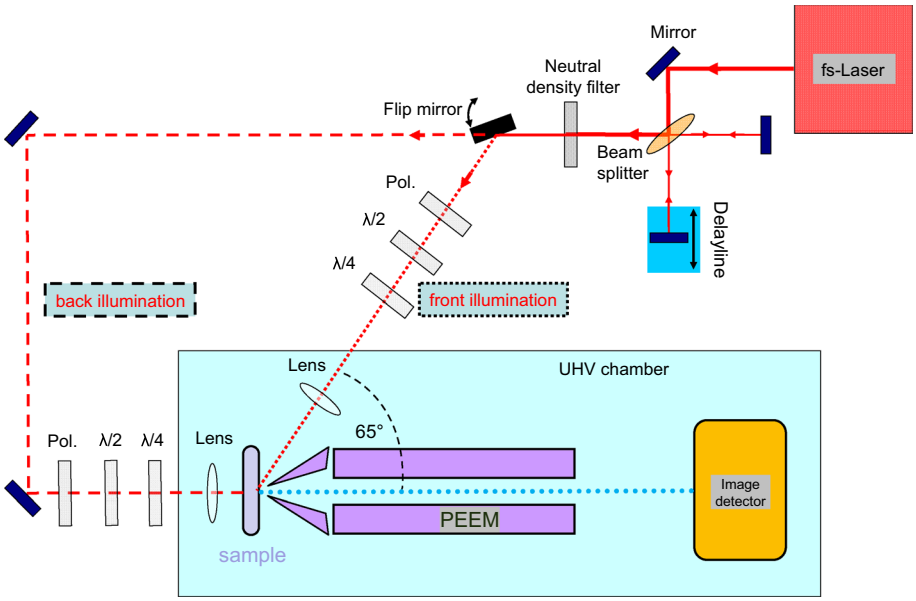

Fig. 2 Illustration of the experimental PEEM setup with front illumination at grazing incidence (usual standard mode of a PEEM) and normal incidence illumination

100 μm. Variation in the polarization is achieved by half- and quarter-wave plates on rotatable mounts. An autocorrelator setup is used for the determination of excitation lifetimes.

3 Results

The photoemission yield I increases with laser power P according to $I \propto P^{\alpha}$ revealing the order α of the photoemission process. Since the photon energy of 1.55 eV is much smaller than the work function of the sample, a higher-order process is necessary. The work function of our sample as measured by photoemission spectroscopy is (4 ± 0.4) eV. This value is larger than the work function of a pristine Au surface (4.8–5.4 eV). We assume that this is caused by a surface contamination from the lithography process or from the sample handling under ambient conditions. In order to exceed the work function, one expects a third-order photoemission process. In this case, a final excitation energy of three times the photon energy is larger than the work function. This is illustrated in the logarithmic plot shown in Fig. 3. The linear fit resulting in a slope of $\alpha = 3.2 \pm 0.5$ confirms the three-photon photoemission (3PPE) process for all measurements discussed here, except for larger laser power where a saturation effect is observed. Please note that the relative emission yields considerably vary for each antenna structure.

Figure 4 shows an exemplary result of a phase-integrated autocorrelation measurement. By dividing the laser beam into two beams of equal intensity using a beamsplitter and merge them after one beam is delayed with respect to the second beam by a variable delay time, we determined the

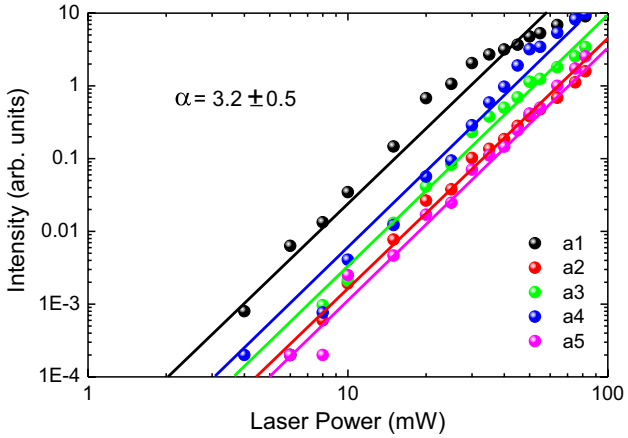

Fig. 3 Double-logarithmic plot of the electron yield as a function of the average laser power revealing a 3PPE process for lower intensities. The polarization was adjusted to linearly polarized light along the x-axis (p-polarization). Data were measured for normal incidence. The linear fit results in a slope α corresponding to the order of the photoemission process

photoemission yield as a function of the delay time. For the 3PPE photoemission process, the photoemission yield results from a third-order autocorrelation of the exciting laser pulse. The ideal third-order autocorrelation of the laser pulse is reproduced by the photoemission yield from the nonresonant channel, whose response is instantaneous. Photoemission from the flat, nonstructured area of the flake approximates instantaneous response as the lifetime of excited photoelectrons far above the Fermi energy represents a few femtoseconds, only [19]. For a Gaussian laser field amplitude, the third-order autocorrelation leads to a Gaussian response function with an increase in its full

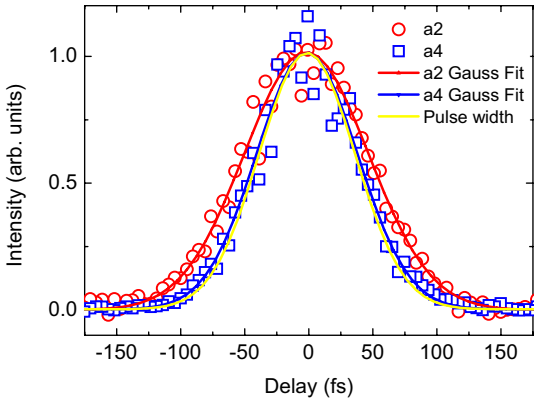

Fig. 4 Exemplary results of the phase-integrated lifetime measurements with linearly polarized light at $\varphi = 90°$ azimuthal angle for antenna a2 (*red*), a4 (*blue*), and flat unstructured Au area (*yellow*) using the autocorrelation technique. The constant background electron yield has been subtracted, and the yields are normalized for comparison

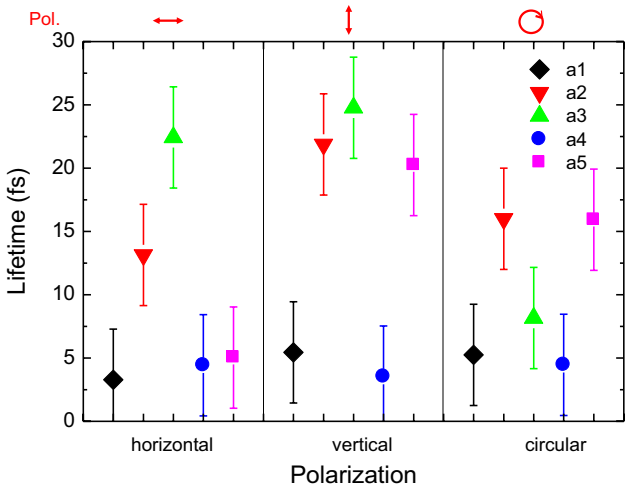

Fig. 5 Lifetime measured for indicated polarization states and antennas. The statistical error is about 4 fs

width at half maximum (FWHM) by a factor of 1.253 [20] with respect to the laser pulse width (in comparison with an increase by $\sqrt{2}$ for a second-order nonlinear process). An intermediate excitation state after the first laser pulse increases the width of the autocorrelation function. This increase corresponds to the lifetime of the intermediate state, which we assume here to be a plasmon excitation. For a quantitative determination of the plasmon lifetime τ_p, we fit the experimental data with a Gaussian function. Figure 4 reveals that the fit with a Gaussian function approximates the experimental data sufficiently well. As a rough approximation, the plasmon lifetime is then calculated according to $\tau_p = (\mathrm{FWHM(ai)} - \mathrm{FWHM(Au)})/1.253$, where FWHM(ai) (FWHM(Au)) corresponds to the fitted FWHM value for antenna ai and flat Au surface. The statistical error of the fit results in a standard deviation of 2 fs. Since τ_p results from a difference of two values, the statistical error amounts to 4 fs. Please note that a numerical simulation considering all excitation channels would be necessary in order to determine correct lifetime values [20].

In particular, antenna a2 shows a large broadening. Values for the lifetimes are depicted for antennas a1–a5 in Fig. 5. Lifetime values are in a range of 5–30 fs which can be expected for localized plasmons in Au nanostructures [21]. The lifetime is typically larger for linear polarization along the *y*-axis (azimuthal angle $\varphi = 90°$) than for linear polarization along the *x*-axis ($\varphi = 0°$). It is expected that a longer lifetime should result in a higher electron yield. Hence, in most cases, these lifetime dependencies of individual antennas can be reconciled well with the normalized electron yields in Fig. 6 for different polarization states. Comparing the photoemission yields for the five investigated antennas at the same polarization state antennas a1 and a4 shows the highest electron yield while a2 and a5 show the lowest near-field enhancement, differing by an order of magnitude. This is in contrast to the expected response from the lifetime measurements where antennas a2 and a5 show comparatively large lifetimes. A tentative explanation for this behavior is that the absolute near-field enhancement is strongly influenced by the real structure of the antennas. Moreover, the arm length is chosen such that antennas a2, a3, and a5 are close to the resonant arm length for 800-nm excitation wavelength while antennas a1 and a4 are out of resonance. Hence, the resonant condition seems to be more important for a long plasmonic lifetime than for the absolute near-field enhancement.

Results for the polarization dependence of the photoelectron yield are shown in Fig. 6. Please note that the exciting electrical field is always in-plane and a phase shift of two orthogonal field components does not occur. The photoemission yield for linear polarization shows a much richer behavior than expected from the fourfold symmetry of the nanoantennas. Obviously, the photoemission yield behaves differently for each individual nanoantenna. Only in the case of the single dipole antenna, one observes the expected maximum yield when the electric field vector points along the long axis of the dipole. The photoemission yield for circular polarization is almost equal to the case of linear polarization along the *x*-axis. Assuming that the photoemission yield is proportional to the third power of the near-field intensity, the observed polarization dependence has been explained by finite-difference time-domain simulations [18]. The variations observed for antennas a1–a4 have been ascribed to nanoscale deviations from the intended symmetric geometry of the cross antennas [18].

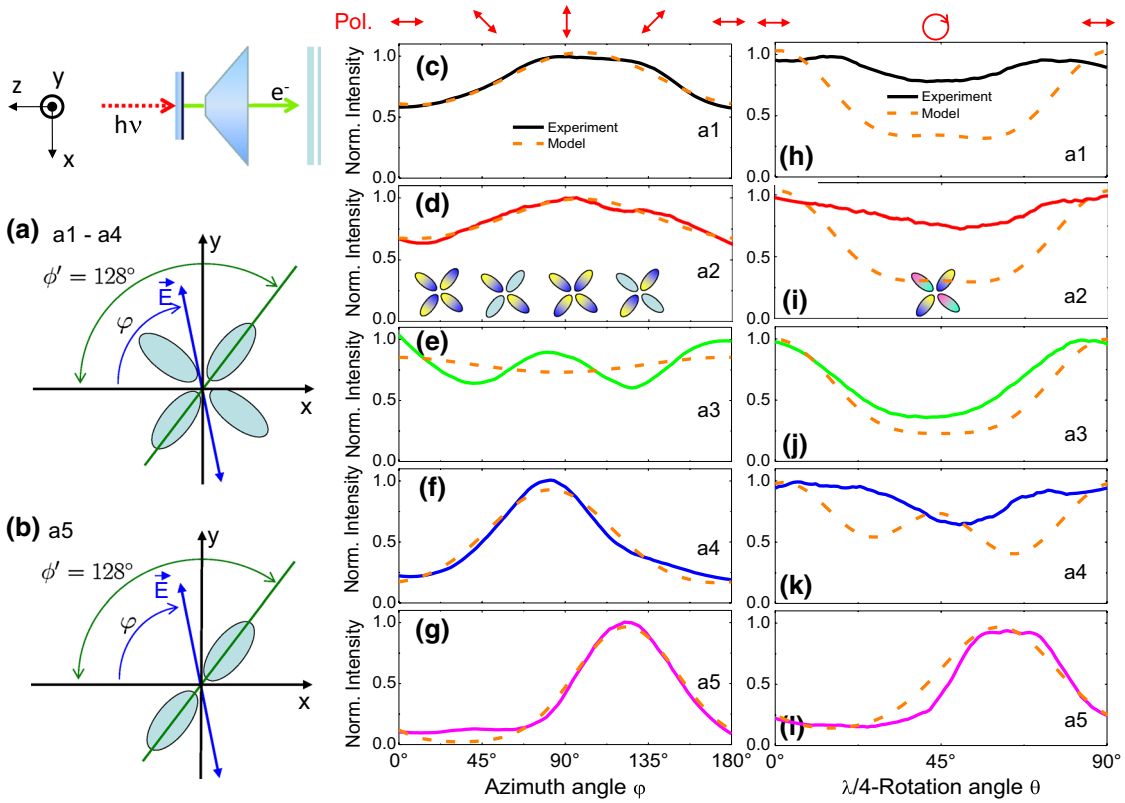

Fig. 6 Photoemission yield for normal incidence illumination of the nanoantennas a1–a5 denoted in Fig. 1. *Top left* Schematic geometry. **a**, **b** Nanoantenna geometry with respect to the horizontal plane as seen from the side of the substrate. **c**–**g** Normalized photoemission yield as a function of azimuthal angle φ for linearly polarized light. **h**, **l** Normalized photoemission yield as a function of the rotation angle θ of the quarter-wave plate. At $\theta = 0°$, the laser light is linearly polarized along the x-axis and at $\theta = 45°$ circularly polarized. *Dashed lines* results of a fit using the components of the response tensor as fit parameters

4 Discussion

In order to understand the response of the cross antennas on the basis of two orthogonal dipole modes, we describe the enhanced field $\mathbf{E}_{nf}$ in the antenna gap by a response tensor $\mathbf{C}$:

$$\mathbf{E}_{nf} = \mathbf{C}\mathbf{E}_i, \tag{1}$$

where $\mathbf{E}_i$ is the incident electrical field, represented in the two-dimensional Jones formalism. Please note that in this case, the distribution of near-field enhancement within the antenna structure is simplified to just two numbers for the two orthogonal components. Perpendicular components of the near field are neglected [22]. For a precise description using finite-difference time-domain simulations, we refer to Ref. [18]. In the case of linear polarized light with the polarization axis rotated by angle φ, the normalized incident field components are given by $E_{i,x} = -\cos\varphi$ and $E_{i,y} = \sin\varphi$. The observable quantity is the electron yield, which is in the case of a 3PPE process related to the third power of the intensity and to the sixth power of the electrical field. The near-field intensity $I_{nf} = |E_{nf,x}|^2 + |E_{nf,y}|^2$ can be directly calculated from Eq. 1. The electron yield I_{e^-} is given by:

$$I_{e^-} \propto \left(|E_{nf,x}|^2 + |E_{nf,y}|^2\right)^3. \tag{2}$$

Using this simplified model, we fit the experimentally observed polarization dependence shown in Fig. 6c–g for each cross antenna (See dashed lines). Fit parameters are the components of the response tensor $C_{i,j}$, ($i = 1, 2$ and $j = x, y$). The two orthogonal dipole modes 1 and 2 may correspond to two orthogonal high symmetry axes of the nanostructure. In the case of an ideal dipole antenna oriented along the x-axis, the response tensor has only one nonzero component $C_{1,x}$. For a rotated ideal dipole antenna along the diagonal as close to the case of antenna a5, one expects

$$\mathbf{C} = \begin{pmatrix} C_{1,x} & C_{1,y} \\ C_{2,x} & C_{2,y} \end{pmatrix} \propto \begin{pmatrix} 1 & 1 \\ 1 & 1 \end{pmatrix} \tag{3}$$

and the ideal cross antenna avoids any oriental preference, i.e., one expects the unit tensor.

Table 1 Fit parameters resulting from a fit of Eq. 2 to the experimentally determined electron yield as a function of the polarization state for antennas a1–a5

	arm l. (nm)	$C_{1,x}$	$C_{1,y}$	$C_{2,x}$	$C_{2,y}$
a1	240	0.92	0.03	0.00	1.00
a2	260	0.94	0.02	0.00	1.00
a3	280	0.97	0.00	0.00	0.94
a4	300	0.98	0.02	0.06	0.75
a5	260	0.39	0.60	0.39	0.60

Please note that the parameter dependence is rather large resulting in a considerable systematic error of the fit result, which we estimated to be of the order of 20 % of the given parameter value

Please note at this point that the model presented here has a weak point as it does not consider differences in the field localization of the two modes. Therefore, the rapid oscillations as observed for example in the case of antenna a3 are not reproduced by the present simple model but fit to numerical simulations.

The comparison of the fit and the experimental data shown in Fig. 6c–g reveals a fair agreement. Fit parameters are summarized in Table 1. The response tensor of antenna a5 is close to the expectation. In the case of antenna a3, showing the highest symmetry in the polarization-dependent electron yield, the response tensor is very close to the unit tensor as expected for an ideal cross antenna.

In the case of circular polarization (see Fig. 6h, l), the quarter-wave-plate rotation causes a smooth transformation from linear polarization to circular polarization and back to linear polarization.

We calculate the polarization of the incident light as a function of the rotation angle θ according to:

$$\mathbf{E}_i(\theta) = \mathbf{R}^{-1} \begin{pmatrix} 1 & 0 \\ 0 & i \end{pmatrix} \mathbf{R} \begin{pmatrix} 1 \\ 0 \end{pmatrix}, \tag{4}$$

with $\mathbf{R}$ denoting the rotation tensor

$$\mathbf{R} = \begin{pmatrix} \cos\theta & \sin\theta \\ -\sin\theta & \cos\theta \end{pmatrix}. \tag{5}$$

The near field $\mathbf{E}_{nf}$ is again calculated by Eq. 1. The photoemission yield I_{e^-} results from Eq. 2, except for a normalization factor, and is shown in Fig. 6h, l. Assuming that the excitation by circular polarization is a linear combination of dipolar modes as described by our simple model, an agreement of experimental and calculated data is expected. This is obviously not the case. The model overestimates the strong reduction in the maximum absolute value of the field vector going from linear to circular polarization. The only cases where this model fits to some extent is the symmetric antenna a3 and the single dipole antenna a5.

5 Summary

Using photoemission microscopy, we have analyzed the photoemission yield of individual lithographically fabricated cross antennas in dependence on the polarization state of the exciting femtosecond laser pulses. We find a dominating 3PPE process to be responsible for the photoemission yield. The photoemission yield reflects the polarization-dependent near-field enhancement. The lifetime of plasmonic excitations is in the order of 5–30 fs. The lifetime shows larger values for resonant wavelengths than in the off-resonant case. This can be expected because for the resonant case, the photoemission yield is prolongated by the excited localized plasmon with long lifetime.

The electron yield was investigated as a function of the polarization for various polarization states for normal incident light. Normal photon incidence leads to a polarization dependence that reflects the symmetry of the antennas. The polarization dependence of the electron yield reveals small deviations from the design structure of individual antennas that are due to the fabrication process.

Tentatively, we describe the dependence of the electron yield on the polarization state by the excitation of two orthogonal dipole modes as motivated by the symmetry of the cross antennas. Only one mode exists for the two-arm antenna. While the rough features can be described by this simple model fairly well, details of the polarization dependence that are caused by the real structure of the antennas require an improved model description based on finite-difference time-domain methods.

Acknowledgments The authors are grateful for financial support from the Deutsche Forschungsgemeinschaft (DFG EL/16-2, SPP1391) and by the Research Center for Complex and Emergent Materials (CINEMA).

References

1. U. Kreibig, M. Vollmer, *Optical Properties of Metal Clusters* (Springer, New York, 1995)
2. D.P. Fromm, A. Sundaramurthy, P.J. Schuck, G. Kino, W.E. Moerner, Gap-dependent optical coupling of single bowtie nanoantennas resonant in the visible. Nano Lett. **4**, 957 (2004)
3. L. Novotny, B. Hecht, *Principles of Nano-optics* (Cambridge University Press, Cambridge, 2006)
4. E. Prodan, C. Radloff, N.J. Halas, P. Nordlander, A hybridization model for the plasmon response of complex nanostructures. Science **302**, 5644 (2003)
5. P. Nordlander, C. Oubre, E. Prodan, K. Li, M.I. Stockman, Plasmon hybridizaton in nanoparticle dimers. Nano Lett. **4**, 899 (2004)
6. P. Nordlander, F. Le, Plasmonic structure and electromagnetic field enhancements in the metallic nanoparticle-film system. Appl. Phys. B **84**, 35 (2006)
7. T. Okamoto, I. Yamaguchi, Optical absorption study of the surface plasmon resonance in gold nanoparticles immobilized onto

a gold substrate by self-assembly technique. J. Phys. Chem. B **107**, 10321 (2003)
8. Y. Uchiho, K. Kajikawa, Evaluation of gap distance between gold nanospheres and a gold substrate by absorption spectroscopy. Chem. Phys. Lett. **478**, 211 (2009)
9. S. Linic, P. Christopher, D.B. Ingram, Plasmonic-metal nanostructures for efficient conversion of solar to chemical energy. Nat. Mater. **10**, 911 (2011)
10. S.F. Heucke, F. Baumann, G.P. Acuna, P.M.D. Severin, S.W. Stahl, M. Strackharn, I.H. Stein, P. Altpeter, P. Tinnefeld, H.E. Gaub, Placing individual molecules in the center of nanoapertures. Nano Lett. **14**(2), 391–395 (2013)
11. C.D. Stanciu, F. Hansteen, A.V. Kimel, A. Kirilyuk, A. Tsukamoto, A. Itoh, T. Rasing, All-optical magnetic recording with circularly polarized light. Phys. Rev. Lett. **99**, 047601 (2007)
12. P. Klaer, F. Schertz, G. Schönhense, H.J. Elmers, Spin-polarized photoelectrons resonantly excited by circularly polarized light from a fractional Ag film on GaAs(100). Phys. Rev. B **88**, 214425 (2013)
13. P. Biagioni, J.S. Huang, L. Duò, M. Finazzi, B. Hecht, Cross resonant optical antenna. Phys. Rev. Lett. **102**, 256801 (2009)
14. R. Mohammadi, A. Unger, H.J. Elmers, G. Schönhense, M.Z. Shushtari, M. Kreiter, Manipulating near field polarization beyond the diffraction limit. Appl. Phys. B **104**, 65 (2011)
15. C. Sönnichsen, T. Franzl, T. Wilk, G. von Plessen, J. Feldmann, O. Wilson, P. Mulvaney, Drastic reduction of plasmon damping in gold nanorods. Phys. Rev. Lett. **88**, 077402 (2002)
16. M.I. Stockman, Nanoscience dark-hot resonances. Nature **467**, 541 (2010)
17. F. Schertz, M. Schmelzeisen, R. Mohammadi, M. Kreiter, H.-J. Elmers, G. Schönhense, Near field of strongly coupled plasmons: uncovering dark modes. Nano Lett. **12**, 1885 (2012)
18. P. Klaer, G. Razinskas, M. Lehr, K. Krewer, F. Schertz, W. Xiao-Fei, B. Hecht, G. Schönhense, H.J. Elmers, Photoemission electron microscopy and finite-element simulation of plasmonic angular momentum confinement in cross resonant optical antennas. Appl. Phys. Lett. **106**, 261101 (2015)
19. M. Bauer, A. Marienfeld, M. Aeschlimann, Prog. Surf. Sci. **90**, 319 (2015)
20. N.E. Karatzas, A.T. Georges, Opt. Commun. **81**, 479 (2006)
21. M. Aeschlimann, T. Brixner, A. Fischer, C. Kramer, P. Melchior, W. Pfeiffer, C. Schneider, C. Struber, P. Tuchscherer, D. Voronine, Science **333**, 1723 (2011)
22. M. Schnell, A. Garcia-Etxarri, J. Alkorta, J. Aizpurua, R. Hillenbrand, Phase-resolved mapping of the near-field vector and polarization state in nanoscale antenna gaps. Nano Lett. **10**, 3524 (2010)